RSC Advances

Preparation of Nano-Ni/meso-Ce-TiO2 by one-step in sol-gel system and their catalytic performance for hydrogenolysis of xylitol

Journal:	*RSC Advances*
Manuscript ID:	RA-ART-05-2015-008472.R2
Article Type:	Paper
Date Submitted by the Author:	04-Aug-2015
Complete List of Authors:	zhou, zhiwei; Nanjing Tech University, College of Chemistry and Chemical Engineering Dai, Songshan; Nanjing Tech University, College of Chemistry and Chemical Engineering Qin, Juan; Productivity Center of Jiangsu Province, Technology and Finance Service Center of Jiangsu Province Yu, Pengcheng; Nanjing Tech University, College of Chemistry and Chemical Engineering Wu, Wen-liang; Nanjing Tech University, College of Chemistry and Chemical Engineering

Journal Name

Paper

Preparation of *Nano*-Ni/*meso*-Ce-TiO_2 by one-step in sol-gel system and their catalytic performance for hydrogenolysis of xylitol

Received 00th January 20xx,
Accepted 00th January 20xx

DOI: 10.1039/x0xx00000x

www.rsc.org/

Zhiwei Zhou[a], Songshan Dai[a], Juan Qin[b], Pengcheng Yu[a], Wenliang Wu*[a]

Abstract: The conventional method for preparation of metal nanoparticle loaded on the mesoporous metal oxide is tedious, and its chemical and physical properties cannot be optionally controlled. A simple and convenient method by one-step in the AcHE sol-gel system was employed for preparation of *nano*-Ni/*meso*-Ce-TiO_2 samples with different Ni nanoparticle loadings. Their physical and chemical properties were characterized by XRD, liquid N_2 adsorption-desorption, EDX, ICP, FT-IR, H_2-TPR and TEM techniques, and their catalytic performance were investigated in the hydrogenolysis of xylitol. The results show that these samples with ordered mesoporous structures, uniform pore size and large specific surface area can be obtained. The Ni nanoparticles can be well dispersed on the mesoporous Ce-TiO_2 surface. The stability of Ni nanoparticles on the mesoporous TiO_2 would be promoted by introduction of little cerium species. The 8% *nano*-Ni/*meso*-Ce-TiO_2 sample shows a higher catalytic performance than other samples. The conversion of xylitol 87.9% amd the total yield of diols 83.2% can be reached. It shows high stability, and the conversion of xylitol and the total yield of diols decreased slightly after repeated reaction for 8 times. The method provides a valuable reference for the preparation of metal nanoparticle loaded on the mesoporous metal oxide, especially for the non-noble metal nanoparticle.

1.Introduction

Metal oxides have been widely applied in the catalysis because of its acid-base, electrical conductivity and oxidation-reduction quality [1]. Compared to the traditional metal oxides, mesoporous metal oxides are more suitable for the catalyst carrier owing to their uniform pore system, which can restrain the aggregation of active constituent dispersed on its surface [2-3]. The mesoporous metal oxides can be successfully templated from nanocrystalline, mesoporous carbon materials, silane-functionalized polymer, organic surfactants and cationic polymers etc [4-10]. The solvent evaporation induced self-assembly process raised by Sanchez et al was regarded as the most effective method for the preparation of mesoporous metal oxides because it can easily control inorganic condensation kinetics of non-silicate mesostructures [11-12]. According to previous reports, a general sol–gel system, including acetic acid, hydrochloric acid and ethanol, which is denoted as AcHE system has been proved to successfully prepare many multicomponent mesoporous metal oxides [13-14].

[a]Chemical Engineering and College of Chemistry and Chemical Engineering, Nanjing Tech University (formerly: Nanjing University of Technology), Nanjing, 210009, P. R. China. E-mail: wwl@njtech.edu.cn
[b]Technology and Finance Service Center of Jiangsu Province, Productivity Center of Jiangsu Province, Nanjing 210042, Pepole's Republic of China. E-mail: qinjuan_1981@163.com

Metal nanoparticles have attracted the extensive attentions due to their smaller particle size and larger special surface area, which are often desired for wide applications in the catalysis, electricity, magnetic and optics regions [15-18]. To improve their catalytic performance, these metal nanoparticles would be dispersed by impregnation or deposition on the carriers including zeolites, mesoporous materials and metal oxides etc [19-22]. Unfortunately, it is hard for the prepared catalysts to work well in practice owing to the aggregation of the pre-synthesized metal nanoparticles. Compared to the catalysts prepared by impregnation or deposition, the pre-synthesized noble metal nanoparticles (Au, Pt and Pd etc) can be dispersed uniformly on the mesoporous metal oxides (SiO_2, ZrO_2, Al_2O_3 and TiO_2 etc) in the AcHE sol-gel system, and the structure of the mesoporous metal oxides would not be affected. Therefore, the method can improve the utilization of noble metal nanoparticles [23] and would provide a new idea for the preparation of nickel based catalysts.

Nickel based catalysts, which were conventionally prepared by impregnation or deposition, are widely used as hydrogenation catalysts because of its low price and high activity. Compared to the noble metal nanoparticles, the Ni nanoparticles are difficult to obtain because the precursor is more difficult to be restored and they would gather easily. Up to now, the reports about the Ni nanoparticles, whose average particle size is less than 6 nm, are quite few [24-26]. On the other hand, the pre-synthesized Ni nanoparticles would be oxidized and assembled after calcination in the AcHE sol-gel system,

and the average particle size of the Ni nanoparticles would not be controlled accurately. Therefore, it is most crucial to develop a method for the preparation of Ni nanoparticles loaded on the mesoporous metal oxides without pre-synthesized Ni nanoparticles, and it is still rarely reported so far.

Diols, such as ethylene glycol (EG), 1,2-propylene glycol (1,2-PG) and 1,3-propylene glycol (1,3- PG), are widely used as pharmaceuticals, liquid fuels, antifreeze agents and solvents [27]. However, the diols are industrially obtained from petroleum feedstocks by the hydration of ethylene oxide or propylene oxide. The catalytic transformation of polyols to diols has attracted considerable attention.

In this work, the Ni nanoparticles uniformly loaded on the ordered mesoporous Ce-TiO_2 samples prepared by one-step in the AcHE sol-gel system were firstly reported, and the chemical physical properties were characterized. Their catalytic performances in the hydrogenolysis of xylitol were investigated.

Fig.1 is the schematic diagram for the preparation of *nano*-Ni/*meso*-Ce-TiO_2 samples by one-step. This facile method is based on a sol−gel process combined with the AcHE system using F127 as the template. In the micellar solution of the titanium precursor, the Ni and Ce precursors could be well dispersed, and F127 can cross-link grow slowly with inorganic precursors in the aging and solvent evaporation processes. After calcination in air and reduction in hydrogen atmosphere, the Ni and Ce could be directly incorporated into mesoporous TiO_2. However, the Ni nanoparticles would be adsorbed on the surface of mesoporous TiO_2 prepared by impregnation, which always results in their aggregation or loss during its application in some reactions.

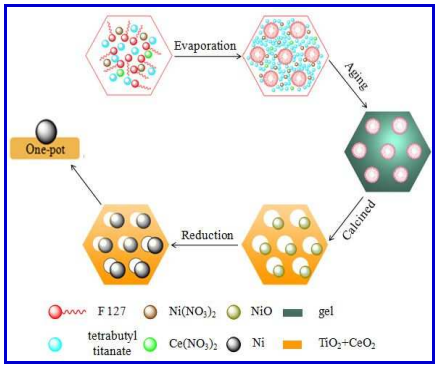

Fig.1 Schematic diagram for the preparation of *nano*-Ni/*meso*-Ce-TiO_2 sample.

2. Experiment

2.1 Sample preparation

Mesoporous TiO_2 sample was synthesized according to the literature[23] using the F127 as a structure-directing agent and tetrabutyl titanate as Ti source. In a typical synthesis process, 1.6 g F127, 1.2 g concentrated hydrochloric acid and 2.4 g acetic acid was diluted into 30ml anhydrous ethanol, and the solution was stirred at 303 K for 10 min to form a transparent solution. After that, 3.4 g tetrabutyl titanate was added into the above solution and stirred for another 2 h at 303 K. The solution was transferred to the Petri dish to evaporate the ethanol at 313 K, and the residual film was aged for 24 h at 338 K. The sample was calcined in air at 623 K for 5 h to remove the organic template and defined as *meso*-TiO_2.

In order to prepare the *nano*-Ni/*meso*-(Ce)-TiO_2 samples, the nickel nitrate ($Ni(NO_3)_2{\cdot}6H_2O$) and cerium nitrate ($Ce(NO_3)_2{\cdot}6H_2O$) were used as Ni and Ce sources, respectively. The *nano*-Ni/*meso*-(Ce)-TiO_2 samples were prepared under the same conditions of *meso*-TiO_2, while tetrabutyl titanate with nickel nitrate and cerium nitrate are added into the solution at the same time. All the samples were reduced at hydrogen atmosphere under appropriate temperature except the samples for H_2-TPR characterization.

For comparison, the sample, defined as 8% Ni/ *meso*-Ce-TiO_2 (IMP), was prepared by impregnation method.

2.2 Material characterization

2.2.1 X-ray powder diffraction analysis

X-ray powder diffraction patterns of the samples were obtained on a Bruker D8 instrument with Ni-filtered Cu Kα radiation (λ=0.154 nm) and operated at 40 kV, 30 mA. The scanning rate was 0.05(º) s^{-1} in the 2θ range from 0.7º to 5º (low-angle XRD) and from 10º to 70º (wide-angle XRD).

2.2.2 Nitrogen adsorption-desorption analysis

Nitrogen adsorption-desorption isotherms of samples were measured at 77 K using a Micromeritics Tristar 3000 system. The surface area was calculated by using the Brunauer-Emmett-Teller (BET) method in the partial pressure (P/P_0) range from 0.01 to 0.99. The mesoporous size distribution was obtained from the adsorption branch of the isotherm by using the Barrett-Joyner-Halenda (BJH) adsorption model.

2.2.3 ICP-OES analysis

The loading of Ni nanopartilces was analyzed by inductively coupled plasma (ICP, Optima2100DV, PerkinElmer, USA) after the sample has been dissolved in HNO_3 solution.

2.2.4 Fourier-transform infrared analysis

Fourier transform infrared spectra were obtained on the Thermo Nicolet NEXUS spectrometer in KBr pellets at room temperature.

2.2.5 Temperature-programmed reduction analysis

Temperature-programmed reduction of hydrogen was carried out in a quartz U-tube reactor, and 300 mg sample was used for each measurement. The sample was pretreated in the argon stream at 623 K for 3 h and then cooled down to room temperature. After that, the mixture of argon and hydrogen was introduced. The temperature was raise from 313 K to 1073 K at a rate of 5 $K{\cdot}min^{-1}$. The consumption of H_2 in the reactant stream was recorded by thermal conductivity detector (TCD).

2.2.6 TEM measurement

The morphology of the samples was visualized using a JEOL JEM 2100 transmission electron microscope (TEM) operated at 120 kV.

The samples were dispersed in ethanol assisted by an ultrasonic technique.

2.2.7 EDX measurement

The dispersion of the elemental composition semiquantitative (Ti, Ce, Ni) were verified by the energy dispersive X-ray spectrometer (EDX) analysis in the Oxford INCA EDAX Detecting Unit.

2.3 Catalytic reaction

The catalytic hydrogenolysis of xylitol was carried out in a 100 ml stainless steel autoclave equipped with a magnetically driven impeller. 0.5 g catalyst was added into the solution of 7.5 g xylitol and 50 ml deionized water. The reactor was flushed for multiple times with hydrogen to replace air. The reaction was carried out at 513 K and 5 MPa for 4 h at a stirring speed 1000 rpm. At the completion of the reaction, the reactor was cooled down to room temperature and the products were collected. The xylitol was analyzed on HPLC equipped with Hyper REZ XP Carbohydrate Ca^{2+} 8 μm column and an ERC RefractoMax 520 detector. The diols were analyzed on a SP-6890 gas chromatograph equipped with a SE-30 column (0.25μm×50m) and a flame ionization detector. The catalytic stability was investigated by filtration without any treatment in the next run.

3.Results and discussion

3.1 Sample Characterization

Fig.2 shows the XRD patterns of *meso*-TiO_2 and *nano*-Ni/*meso*-TiO_2 samples with different Ni nanoparticle loadings. From Fig.2, it can be seen that the *meso*-TiO_2 sample shows typical anatase tetragonal crystal structure and its crystallite size is about 7.5 nm calculated by Scherrer equation [28], which is much smaller than commercial TiO_2 samples. For different *nano*-Ni/*meso*-TiO_2 samples, the characteristic diffraction peak corresponding to the Ni (111) phases [29] are present in the all samples, whose intensity increases with the Ni nanoparticle loading increasing. For the 8% *nano*-Ni/*mseo*-TiO_2 sample, its crystallite size of TiO_2 and Ni nanoparticles is about 8.5 and 19.4 nm calculated by Scherrer equation, respectively.

In order to reduce the crystallite size of Ni nanoparticles, cerium species was introduced into *nano*-Ni/*meso*-TiO_2 samples [30-31]. XRD patterns, N_2 adsorption-desorption and pore size distributions of *meso*-Ce-TiO_2 and *nano*-Ni/*meso*-Ce-TiO_2 samples are shown in Fig.3. Compared to the 8% *nano*-Ni/*meso*-TiO_2 sample, it can be seen from Fig.3 (A) that the characteristic diffraction peak corresponding to the Ni (111) phases for the 8% *nano*-Ni/*meso*-Ce-TiO_2 sample became wider and could be ignored owing to the smaller crystallite size of Ni nanoparticles, which is about 8.5 nm calculated by Scherrer equation. A strong peak around 1° from Fig.3 (B) and typical type-IV N_2 adsorption-desorption isotherms from Fig.3 (C) can be observed for all the samples, suggesting their hexagonal ordered mesoporous structure [29]. With the increasing of the Ni nanoparticle loading, the peak would be shifted to higher

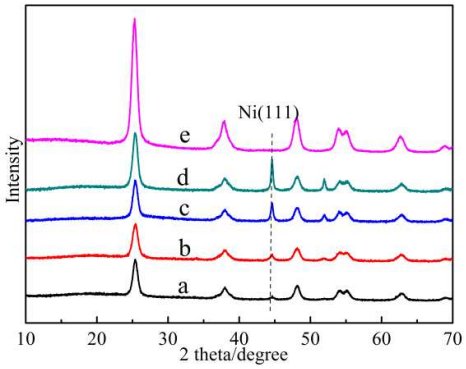

Fig.2 XRD patterns for (a)4% *nano*-Ni/*meso*-TiO_2, (b)8% *nano*-Ni/*meso*-TiO_2, (c)12% *nano*-Ni/*meso*-TiO_2, (d)16% *nano*-Ni/*meso*-TiO_2, (e)*meso*-TiO_2 samples.

degree, which indicates that the interplanar spacing decreased on the basis of the Bragg equation [32]. The physical properties for all the samples are listed in Table 1. It can be seen that the samples have a large surface area, pore volume and size, which is beneficial to its catalytic performance, although there is a decrease with the increasing of Ni nanoparticle loading.

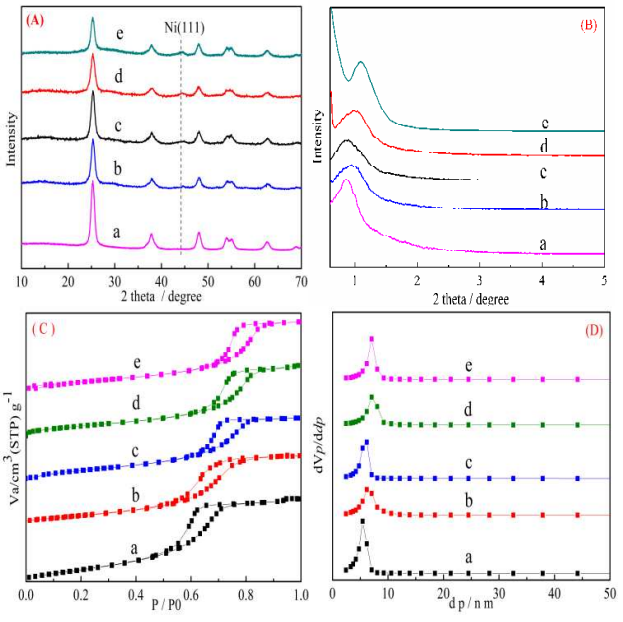

Fig.3 (A) wide-angle XRD patterns, (B) low-angle XRD patterns, (C) N_2 adsorption-desorption isotherms and (D) pore size distributions for (a) *meso*-Ce-TiO_2, (b) 2% *nano*-Ni/*meso*-Ce-TiO_2, (c) 4% *nano*-Ni/*meso*-Ce-TiO_2, (d) 6% *nano*-Ni/*meso*-Ce-TiO_2, (e) 8%*nano*-Ni/*meso*-Ce-TiO_2 samples.

Table 1 Physical properties for (a)*meso*-Ce-TiO_2, (b)2% *nano*-Ni/*meso*-Ce-TiO_2, (c)4% *nano*-Ni/*meso*-Ce-TiO_2, (d)6% *nano*-Ni/*meso*-Ce-TiO_2, (e) 8% *nano*-Ni/*meso*-Ce-TiO_2.

Samples	D_p/(nm)	S_{BET} /($m^2 \cdot g^{-1}$)	V_p/($cm^3 \cdot g^{-1}$)	Loading / (wt %)
a	5.1	214.7	0.30	0.0
b	5.0	180.4	0.28	1.99
c	4.9	155.0	0.26	4.01
d	4.9	147.6	0.25	5.97
e	4.8	137.5	0.23	7.84

The calcination temperature would affect severely the interaction of the components of the samples [33]. The influence of calcination temperature on the structure of the 8% *nano*-Ni/*meso*-Ce-TiO_2 was carried out, and their XRD patterns are shown in Fig.4. When the calcination temperature increased up to 723 K, the diffraction peak corresponding to Ni (111) can be obviously observed, and the peak intensity would be promoted with the calcination temperature increasing, which indicates that some bulk aggregates of Ni specieswere formed. The average crystallite size of Ni nanoparticles calculated by Scherrer equation was listed in the Table 2. When the calcination temperature was 673 K, the average crystallite size of Ni nanoparticles was smaller than others, which is about 8.5 nm. Although the calcination temperature are the same, compared to the sample f, the characteristic diffraction peak corresponding to Ni (111) for sample a is boarder, which can conclude that the crystallite size of Ni nanoparticles would be reduced by introduction of little cerium species.

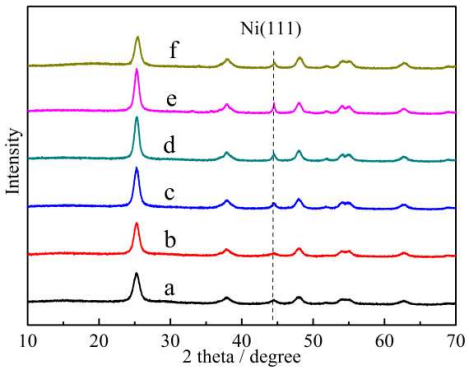

Fig.4 XRD patterns for 8% *nano*-Ni/*meso*-Ce-TiO_2 under different calcination temperatures (a) 623 K, (b) 673 K, (c) 723 K, (d) 773 K, (e) 823 K and (f) 8% *nano*-Ni/*meso*-TiO_2 calcined at 623 K.

.

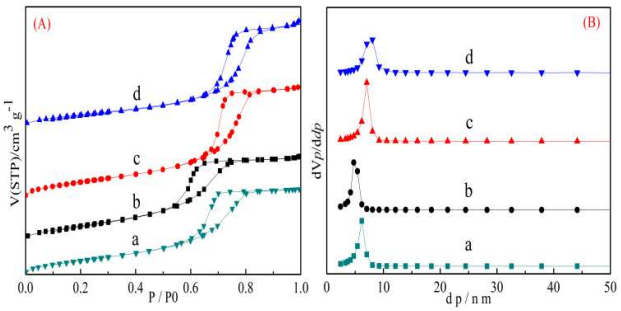

Fig.5 Liquid N_2 adsorption-desorption isotherms (A) and pore size distribution (B) for 8% *nano*-Ni/*meso*-Ce-TiO_2 under different calcination temperatures (a) 623 K, (b) 673 K, (c) 723 K, (d) 773 K.

Table 2 Physical properties for 8% *nano*-Ni/*meso*-Ce-TiO_2 under different calcination temperatures (a) 623 K, (b) 673 K, (c) 723 K, (d) 773 K.

Samples	D_p/(nm)	S_{BET} /($m^2 \cdot g^{-1}$)	V_p/($cm^3 \cdot g^{-1}$)	D_{Ni}/(nm)
a	6.2	126.6	0.23	10.2
b	4.8	137.5	0.23	8.5
c	7.1	123.0	0.22	16.6
d	8.1	105.0	0.20	21.2

The liquid N_2 adsorption-desorption isotherms and pore size distribution for 8% *nano*-Ni/*meso*-Ce-TiO_2 sample under different calcination temperature are shown in Fig.5, and the physical properties are listed in Table 2. All the samples can keep its mesoporous character well, and their pore size is uniform. From Table 2, the pore size from 6.2 nm to 4.8 nm and the surface area from 126.6 $m^2 \cdot g^{-1}$ to 137.5 $m^2 \cdot g^{-1}$ can be obtained when the calcination temperature increase from 623 K to 673 K, which may be owing to the stronger interaction between Ni nanoparticles and *meso*-Ce-TiO_2 carrier resulting in the increasing of the Ni nanopartilces dispersity [33]. However, with the further increasing of calcination temperature, the surface area decreased, which would be attribute to the sintering of TiO_2 probably [34]. Therefore, the appropriate calcination temperature for 8% *nano*-Ni/*meso*-Ce-TiO_2 sample is 673K.

In order to understand the nature of Ni nanoparticles clearly, the H_2-TPR, SEM, TEM and FT-IR techniques were utilized. The H_2-TPR profiles of different samples are shown in Fig.6. One major peak between 627 K and 716 K was observed for samples a-f prepared by one-pot method, which was assigned to the reduction of NiO interacted with the carrier [35-36]. Compared to the sample a, the peak for sample b was shifted to higher temperature because of the stronger interaction, which implied that the introduction of little cerium species can increase the dispersion of Ni nanoparticles [37]. At the same time, the interaction was strengthened with the calcination temperature increasing. Two major peaks, one at 553 K

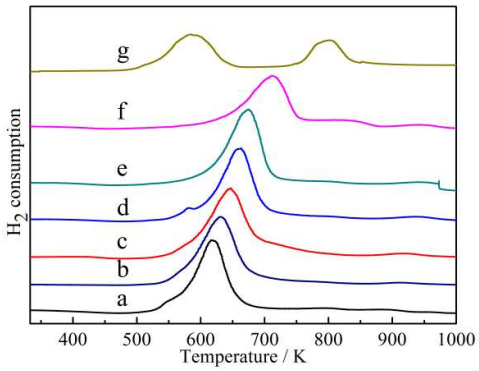

Fig.6 H_2-TPR profiles for (a) 8% *nano*-Ni/*meso*-TiO_2 calcined at 623 K, 8% *nano*-Ni/*meso*-Ce-TiO_2 under different calcination temperatures (b) 623 K, (c) 673 K, (d) 723 K, (e) 773 K, (f) 823 K and (g) 8% Ni/*meso*-Ce-TiO_2 (IMP).

and another at 818 K were observed for sample g prepared by impregnation method, which is owing to the reduction of bulk NiO and NiO interacted with the carrier, respectively. It can be concluded that the Ni nanoparticles are not uniformly dispersed by impregnation method [38].

The SEM photos and election mapping of particles for 8% nano-Ni/meso-Ce-TiO_2 sample are shown in Fig.6. As displayed in Fig.7 (a), the granular morphology was obtained. It can be seen from Fig.7 (b-d) that the EDX element mapping showed uniform X-ray intensities of Ni and Ce signals, suggesting its homogeneous distribution of the Ni nanoparticles in the *meso*-Ce-TiO_2 matrix [39], which agrees to the XRD analysis.

Fig.8 is the TEM images for 8% *nano*-Ni/*meso*-Ce-TiO_2 sample calcined at 673 K. From Fig.8 (A), the typical ordered mesostructure was obviously observed, which was in good agreement with the intense XRD peak at low angle. Additional proof for the crystallinity

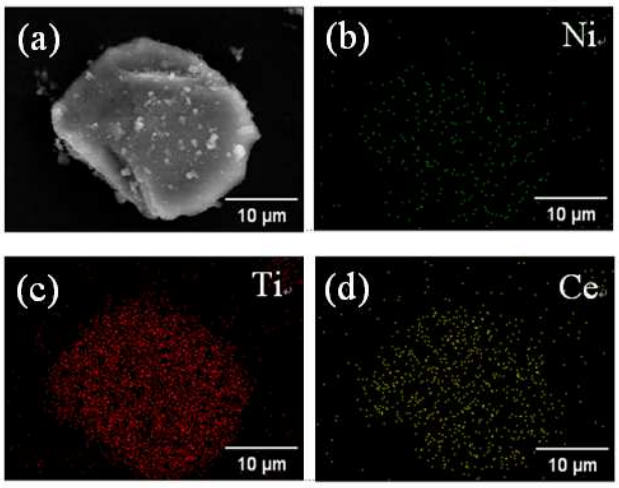

Fig.7 The SEM photo (a) and election mapping of particles (b-d) for the 8% *nano*-Ni/*meso*-Ce-TiO_2 sample calcined at 673K.

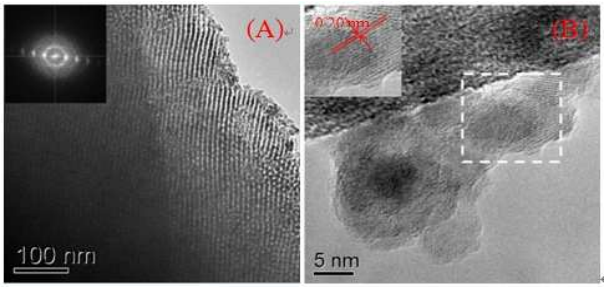

Fig.8 TEM images for 8% *nano*-Ni/*meso*-Ce-TiO_2 sample calcined at 673 K.

of the framework walls is given by high-resolution TEM image (B). The (111) planes can be identified by the typical interfringe distance of 0.20 nm, which is close to the lattice spacing of the (111) planes of the face-centered cubic Ni crystal (0.203nm). It reveals that several crystalline Ni nanoparticles with well-defined lattice planes are exist [40-41].

FT-IR spectra of different samples are shown in Fig.9. The bands between 400 and 900 cm^{-1} could be assigned to the stretching vibration of Ti-O bond [42]. Compared to the sample a, a new band about at 1300 cm^{-1}, which is attribute to the emergence of Ti-O-M (M = metal ions), are observed for other three samples when the cerium or nickel species are introduced. It can be concluded that the cerium or nickel species can be inserted into the framework of the mesoporous TiO_2 sample [42-45].

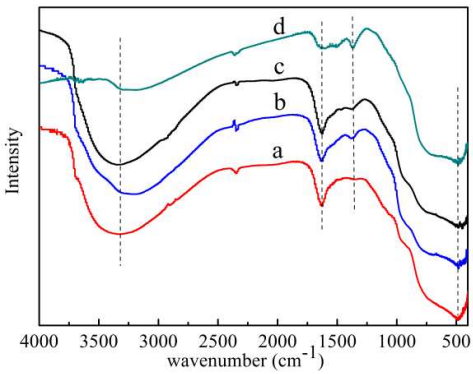

Fig.9 FT-IR spectra for (a)*meso*-TiO_2, (b)*meso*-Ce-TiO_2, (c)8% *nano*-Ni/*meso*-TiO_2, (d)8% *nano*-Ni/*meso*-Ce-TiO_2.

3.2 Catalytic Performance of different catalysts for hydrogenolysis of xylitol

Catalytic performances of different catalysts in the hydrogenolysis of xylitol are listed in Table 3. From Table 3, it can be seen that with the Ni nanoparticle loading increasing from 2% to 8%, the conversion of xylitol increased. The most active catalyst was 8% *nano*-Ni/*meso*-Ce-TiO_2, giving a xylitol conversion of 87.9% and a diols total yield of 83.2%. However, although the Ni species loading is the same, the catalytic performance of 8% *nano*-Ni/*meso*-Ce-TiO_2

sample prepared by one-pot method is much higher than 8% Ni/*meso*-Ce-TiO_2 (IMP) sample prepared by impregnation method, which shows a xylitol conversion of 74.5% and a diols total yield of 68.2%, respectively. The results demonstrated the superior ability of the one-pot method for dispersing/incorporating Ni nanoparticles into the mesoporous TiO_2.

Table 3 Catalytic performance of different catalysts in the hydrogenolysis of xylitol.

catalysts	Conversion /%	Yield/%			Y_{total} /%
		EG	1,2-PDO	1,3-PDO	
2% *nano*-Ni /*meso*-Ce-TiO_2	42.1	21.8	6.1	2.8	30.7
4% *nano*-Ni /*meso*-Ce-TiO_2	61.3	34.7	10.9	6.5	52.1
6% *nano*-Ni /*meso*-Ce-TiO_2	77.3	45.5	11.8	12.9	70.2
8% *nano*-Ni /*meso*-Ce-TiO_2	87.9	50.2	17.0	16.0	83.2
8% Ni /*meso*-Ce-TiO_2 (IMP)	74.5	41.4	14.9	11.9	68.2

The catalytic stability for 8% *nano*-Ni/*meso*-Ce-TiO_2 and 8% Ni/*meso*-Ce-TiO_2 (IMP) catalysts in the hydrogenlysis of xylitol was investigated, and the results are shown in Fig.10. It can be seen the total yield of diols decreased slightly, and it can reach about 78.7% after repeated reaction for 8 times, which suggested that catalytic stability keeps well. However, the total yield of diols decreased severely, and it is only 31.9% after repeated reaction for 8 times for the 8% Ni/*meso*-Ce-TiO_2 (IMP), which may be owing to the loss of the Ni species.

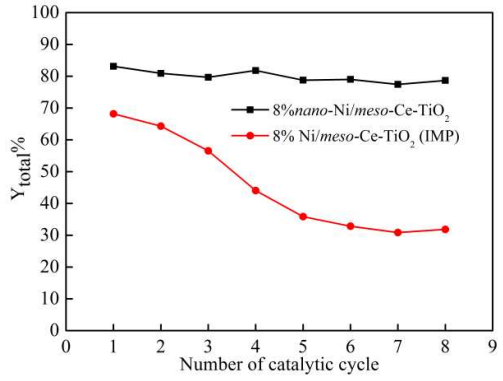

Fig.10 Catalytic stability for 8% *nano*-Ni/*meso*-Ce-TiO_2 and 8% Ni/*meso*-Ce-TiO_2 (IMP) catalysts in the hydrogenlysis of xylitol.

4.Conclusions

Ni nanoparticles well-dispersed on the *meso*-Ce-TiO_2 by one-step in the AcHE sol-gel system has been developed in this article and investigated in the hydrogenolysis of xylitol. Characterization results revealed that the prepared samples possessed an order mesoporous character. Meanwhile, a little cerium species introduced into the *meso*-TiO_2 can increase the stability of Ni nanoparticles and reduce the crystallite size of Ni nanoparticles. The catalytic performance of 8% *nano*-Ni/*meso*-Ce-TiO_2 was much higher than 8% Ni/*meso*-Ce-TiO_2 (IMP) although their Ni species loading is the same. The catalytic stability for 8% *nano*-Ni/*meso*-Ce-TiO_2 keeps well, and the total yield of diols is 78.7% after repeated reaction for 8 times. The method can provide a guide for preparation non-noble metal catalysts with high catalytic performance and make these samples to be a good application prospect.

Acknowledgements

This work was supported by Jiangsu Planned Projects for Postdoctoral Research Funds (1302121C); Open Project of Beijing Key Laboratory for Enze Biomass and Fine Chemicals; Project Funded by the Priority Academic Program Development of Jiangsu Higher Education Institutions.

Notes and references

(1) Y. Ren, Z. Ma and P. G. Bruce, *Chem. Soc. Rev*., 2012, **41**, 4909-4927.
(2) R. Y. Zhang, A. A. Elzatahry, S. S. Al-Deyab and D. Y. Zhao, *Nano Today*, 2012, **7**, 344-366.
(3) A. Corma, *Chem. Rev*., 1997, **97**, 2373-2419.
(4) J. S. Beck, J. C. Vartuli, W. J. Roth, M. E. Leonowicz, C. T. Kresge, K. D. Schmitt, C. T. W. Chu, D. H. Olson, E. W. Sheppard, S. B. McCullen, J. B. Higgins and J. L. Schlenker, *J. Am. Chem. Soc*., 1992, **114**, 10834-10843.
(5) C. T. Kresge, M. E. Leonowicz, W. J. Roth, J. C. Vartuli and J. S. Beck, *Nature*, 1992, **359**, 710-712.
(6) A. Firouzi, D. Kumar, L. M. Bull, T. Besier, P. Sieger, Q. Huo, S. A. Walker, J. A. Zasadzinski, C. Glinka, J. Nicol, D. Margolese, G. D. Stucky and B. F. Chmelka, *Science*, 1995, **267**, 1138-1143.
(7) F. Jiao and P. G. Bruce, *Angew. Chem., Int. Ed*., 2004, **43**, 5958-5961.
(8) J. Roggenbuck and M. Tiemann, *J. Am. Chem. Soc*., 2005, **127**, 1096-1097.
(9) M. Kang, D. Kim, S. H. Yi, J. U. Han, J. E. Yie and J. M. Kim, *Catal. Today*, 2004, **93**, 695-699.
(10)S. Polarz, A. V. Orlov, F. Schuth and A. H. Lu, *Chem. -A Eur. J*., 2007, **13**, 592-597.
(11)C. J. Brinker, Y. F. Lu, A. Sellinger and H. Y. Fan, *Advanced Materials*, 1999, **11**, 579-585.
(12)D. Grosso, F. Cagnol, G. Soler-Illia, E. L. Crepaldi, H. Amenitsch, A. Brunet-Bruneau, A. Bourgeois and C. Sanchez, *Adv. Funct. Mater*., 2004, **14**, 309-322.
(13)J. Fan, S. W. Boettcher and G. D. Stucky, *Chem. Mater*., 2006, **18**, 6391-6396.
(14)Y. H. Dai, X. Q. Yan, Y. Tang, X. N. Liu, L. P. Xiao and J. Fan, *ChemCatChem*., 2012, **4**, 1603-1610.
(15)B. H. Kim, M. J. Hackett, J. Park and T. Hyeon, *Chem. Mater*., 2014, **26**, 59-71.
(16)L. H. Reddy, J. L. Arias, J. Nicolas and P. Couvreur, *Chem. Rev*., 2012, **112**, 5818-5878.

(17)P. Claus, A. Bruckner, C. Mohr and H. Hofmeister, *J. Am. Chem. Soc*., 2000, **122**, 11430-11439.

(18)S. Carenco, Y. Hu, I. Florea, O. Ersen, C. Boissiere, N. Mezailles and C. Sanchez, *Chem. Mater*., 2012, **24**, 4134-4145.

(19)C. H. Christensen, K. Johannsen and I. Schmidt, *J. Am. Chem. Soc*., 2003, **125**, 13370-13371.

(20)Y. J. Han, J. M. Kim and G. D. Stucky, *Chem. Mater*., 2000, **12**, 2068-2069.

(21)M. Wang, F. Wang, J. P. Ma, C. Chen, S. Shi and J. Xu, *Chem. Commun*., 2013, **49**, 6623-6625.

(22)M. Wang, F. Wang, J. P. Ma, M. Li, Z. Zhang, Y. H. Wang, X. C. Zhang and J Xu, *Chem. Commun*., 2014, **50**, 292-294.

(23)J. J. Liu, S. H. Zou, S. Li, X. F. Liao, Y. J. Hong, L. P. Xiao and J. Fan, *J. Mater. Chem. A*, 2013, **1**, 4038-4047.

(24)S. Tomiyama, R. Takahashi, S. Sato, T. Sodsawa and S. Yoshida, *Appl. Catal. A*, 2003, **241**, 349-361.

(25)S. Alkhaldi and M. M. Husein, *Energy Fuels*, 2014, **28**, 643-649.

(26)M. F. Calderon, E. Zelaya, G. A. Benitez, P. L. Schilardi, A. H. Creus, A. G. Orive, R. C. Salvarezza and F. J. Ibanez, *Langmuir*, 2013, **29**, 4670-4678.

(27) A. M. Ruppert, K. Weinberg, and R. Palkovits, *Angew. Chem. Int. Ed*., 2012, **51**, 2564 – 2601.

(28)Y. H. Dai, X. Q. Yan, Y. Tang, X. N. Liu, L. P. Xiao and J. Fan, *ChemCatChem*., 2012, **4**, 1603-1610.

(29)L. L. Xu, H. L. Song and L. J. Chou, *ACS Catal*., 2012, **2**, 1331-1342.

(30)D. Andreevaa, I. Ivanova, L. Ilievaa and M. V. Abrashev, *Appl. Catal. A,* 2006, **302**, 127-132.

(31)C. Daza, A. Kiennemann, S. Moreno and R. Molina, *Energy Fuels*, 2009, **23**, 3497-3509.

(32) Y. F. Zhu, X. Kong, X. Q. Li, G. Q. Ding, Y. L. Zhu and Y. W. Li, *ACS Catal*., 2014, **4**, 3612−3620.

(33)S. Badoga, R. V. Sharma, A. K. Dalai and J. Adjaye, *Ind. Eng. Chem. Res*., 2014, **53**, 18729-18739.

(34)N. Yao, J. X. Chen, J. X. Zhang and J. Y. Zhang, *Catal. Commun*., 2008, **9**, 1510-1516.

(35)J. X. Chen, N. Yao, R. J. Wang and J. Y. Zhang, *Chem. Eng. J*., 2009, **148**, 164-172.

(36)M. J. Lazaro, Y. Echegoyen, C. Alegre, I. Suelves, R. Moliner and J. M. Palacios, *Int. J. Hydrogen Energy*, 2008, **33**, 3320-3329.

(37)F. H. Meng, Z. Li, J. Liu, X.X. Cui and H.Y. Zheng, *J. Nat. Gas Sci. Eng*., 2015, **23**, 250-258.

(38)K. Wang, X. J. Li, S. F. Ji, X. J. Shi and J.J. Tang, *Energy Fuels,* 2009, **23**, 25-31.

(39)J.J. Liu, X. P. Wu, S.H. Zou, Y.H. Dai, L.P. Xiao, X. Q. Gong and J. Fan, *J. Phys. Chem. C*, 2014, **118**, 24950–24958.

(40)P. Li, J. Y. Liu, N. Nag and P. A. Croziers, *J. Phys. Chem. B*, 2005, **109**, 13883-13890.

(41)O. Metin, V. Mazumder, S. Ozkar and S. S. Sun, *J. AM. Chem. Soc*., 2010, **132**, 1468-1469.

(42)Y. Xu, J. Q. Ma, Y. F. Xu, H. Li, H. X. Li, P. Li and X. G. Zhou, *Appl. Catal. A*, 2012, **413**, 350-357.

(43)C. Daza, A. Kiennemann, S. Moreno and R. Molina, *Energy Fuels*, 2009, **23**, 3497-3509.

(44)P. Li, Y. Xin, Q. Li, Zh. P. Wang, Zh. L. Zhang and L. R. Zheng, *Environ. Sci. Technol*. 2012, **46**, 9600−9605.

(45)Y. X. Zhang, G. H. Li, Y. C. Wu, Y. Y. Luo and L. D. Zhang, *J. Phys. Chem. B*, 2005, **109**, 5478-5481.

Highlight:

Preparation of *Nano*-Ni/*meso*-Ce-TiO_2 by one-step in sol-gel system and their catalytic performance for hydrogenolysis of xylitol

Zhiwei Zhou[a], Songshan Dai[a], Juan Qin[b], Pengcheng Yu[a], Wenliang Wu*[a]

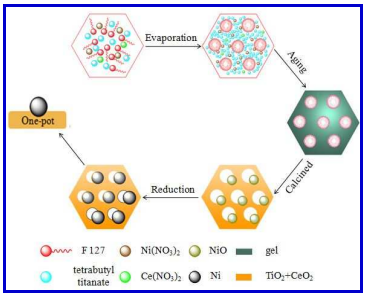

Nano-Ni/*meso*-Ce-TiO_2 samples with good catalytic performance were successfully synthesized via one-step in the AcHE sol-gel system.